

RESEARCH PAPER

## A novel three-dimensional printing of electroconductive scaffolds for bone cancer therapy application

Marjan Monshi<sup>1</sup>, Saeid Esmaili<sup>2</sup>, Amin Kolooshani<sup>2</sup>, Bahareh Kamyab Moghadas<sup>3\*</sup>,  
Saeed Saber-Samandari<sup>4</sup>, Amir-salar Khandan<sup>4\*\*</sup>

<sup>1</sup>Advanced Materials Research Centre, Department of Materials Science and Engineering, Najafabad Branch, Islamic Azad University, Najafabad, Iran

<sup>2</sup>Mechanical Engineering Department, Khomeinishahr Branch, Islamic Azad University, Khomeinishahr, Iran

<sup>3</sup>Department of Chemical Engineering, Shiraz Branch, Islamic Azad University, Shiraz, Iran

<sup>4</sup>New Technologies Research Center, Amirkabir University of Technology, Tehran, 15875-4413, Iran

### ABSTRACT

**Objective(s):** Tissue engineering aims to achieve a tissue, which has highly interconnected porous microstructure concurrent with appropriate mechanical and biological properties.

**Materials and Methods:** Therefore, the microstructure scaffolds are of great importance in this field. In the present study, an electroconductive poly-lactic acid (EC-PLA) filament used to fabricate a porous bone scaffold. For scaffolds model designed, solid-work software was used. Then, the designed modeled was transferred to simplify 3D to laminated with its G-Code file for fused deposition modeling (FDM) printer to create a scaffold with porosity around 65-75%. Two different shapes were designed and fabricated (cylindrical and cubic shape). The samples were coated with hydroxyapatite (HA) nanoparticle to enhance its chemical stability. In this study, the X-ray diffraction (XRD) confirmed that the EC-PLA is non-crystallized and scanning electron microscopy (SEM) used to present the apatite formation on the surface of porous scaffolds. The compression test, fracture toughness, and hardness were measured. The biological response in the physiological saline was performed to determine the rate of degradation of EC-PLA in phosphate buffer saline (PBS) and the apatite formation in the simulated body fluid (SBF) after 14 days.

**Results:** Finally, the biocompatibility of the porous architecture was monitored using human gum (HuGu) cells. The ABAQUS modeling simulation was used to compare the experimental and analytical results. The obtained results showed that by applying force to both cylindrical and cubic scaffold, the Von Mises Stress (VMS) could withstand the scaffold mentioned above at 9.7-11 MPa.

**Conclusion:** Therefore, it can be concluded that prepared porous scaffolds have a high potential in bone tissue engineering and probably the treatment of tumor-related bone defects as photothermal therapy. The porous EC-PLA scaffold was successfully fabricated and showed appropriate compressive strength (39.14 MPa), with controllable porosity of 60-70 %, which is a suitable candidate for replacing in bone tissues.

**Keywords:** Cell culture, Electroconductive Poly lactic acid, Scaffold, Tissue engineering

### How to cite this article

Monshi M, Esmaili S, Kolooshani A, Kamyab Moghadas B, Saber-Samandari S, Khandan A. A novel three-dimensional printing of electroconductive scaffolds for bone cancer therapy application. *Nanomed J.* 2020; 7(2): 138-148. DOI: 10.22038/nmj.2020.07.007

### INTRODUCTION

Different bone repair and transplantation replacement have obtained with the development of material technology. Tissue engineering has made into the extracellular matrix (ECM) scaffold, which is an interdisciplinary field, assists cell

therapy by using a scaffold, cell, and growth factor [1]. Tissue engineering for bone regeneration has desirable characteristics with biocompatibility, non-toxicity, low cost, and non-carcinogenicity, with excellent osteoconductive and osteoinductive properties. Several approaches such as pore-forming agent method [2], supercritical method [3,4] gas foaming method [5, 6], sol-gel method [7, 8], and freezing drying [9, 10], 3D printing [11-15] have developed to obtain porous

\* Corresponding Author Email: [amir\\_salar\\_khandan@yahoo.com](mailto:amir_salar_khandan@yahoo.com)  
[kamyab@iaushiraz.ac.ir](mailto:kamyab@iaushiraz.ac.ir)

Note. This manuscript was submitted on December 6, 2019; approved on February 27, 2020

scaffolds for bone tissue replacement to mimic human bone mass density (BMD) using bone remodeling drug like vitamin D. Although these methods exhibit a particular ability to fabricate porous nanostructure, they are also with some limitations, such as inaccurate control of the pore structure and poor ability to customize for specific defect sites [11]. Some of this path inevitably leave organic residues of pore-forming agent that reduce the biological properties of scaffolds and atonement the quality of bone repair [11-13].

Achieving various fabrication techniques that can obtain significant external shape and control the pore structure accurately for orthopedic application. Additive manufacturing (AM) can produce a porous scaffold with individual external shape and porous internal microstructure [12]. The 3D printing (3DP) technology has the advantage techniques a precise, personalized tissue for bone scaffolds based on bone defect and CT-scan images. The results indicated that matching the scaffold with the defect areas excellently, imitate the normal nature tissue microstructure of humans is possible within the AM technology [13-14]. A large variety of ceramic, metallic, polymeric, and composite materials can be processed using 3DP; however, binder selection and process parameter optimization are the keys to successful part fabrication. In bone tissue engineering, the advantages of this method arise through the control of fine features, including interconnected porosity, no contamination issues related to any second material for support structures, and the direct printing ability with both metallic and ceramic biomaterials [15]. Serra et al. [16] used a nozzle-based rapid prototyping system to combine polylactic acid (PLA) and bioactive calcium phosphates (CaPs) to fabricate 3D porous scaffolds architecture. The investigations resulted in acceptable suitability of the techniques - materials combination lead to developing 3D porous scaffolds and their initial biocompatibility, both being valuable characteristics for bone tissue engineering approaches. An *in vitro* study compared three different poly (D, L-lactic acid) scaffolds obtained by various pore sizes generated by applying different salt leaching processes. Researchers found that different pore size matrixes can affect ECM development, the cell organization, collagen, and mineralization correlation. They focused on the intermediate stage of the bone healing

process, where a collagen network is beginning to develop by the growing osteoblasts representing the cite for the ultimate stage of bone formation [17]. Giordano et al. [18] fabricated scaffold by binder printed from low and high molecular weight PLA granules with chloroform used as a binder solution. The maximum tensile strength for the low molecular weight PLLA was  $17.40 \pm 0.71$  MPa, and for high molecular weight, PLLA was  $15.94 \pm 1.50$  MPa. Another study investigated different properties of PLA scaffolds fabricated using 3DP technology. Their result showed that there is a similarity between 3D-printed scaffolds and natural bone in terms of pore size, porosity, and appropriate mechanical properties of porous tissues. Thus, it would be a suitable alternative for the bone repairing process [19]. Fafenrot et al. [20] demonstrate that hybrid materials mostly containing bronze have significantly reduced mechanical properties of metal-polymer scaffolds. The tensile strengths of the 3D-printed objects were near with those original bone, which indicated sufficient quality of the printing process. They showed that while Fusion Deposition Modelling (FDM) allows for producing objects with mechanical properties similar to the original materials, metal-polymer blends could not be used for the rapid manufacturing of objects requiring proper mechanical strength. Many studies showed that graphene had potential biological properties and could improve the adhesion, proliferation, and differentiation of osteoblasts. Also, in some cases, the obtained results indicated that graphene had marvelous potential in bone repair [21]. However, there are still some shortcomings of graphene, electroconductive, magnetic nanoparticle, and carbon nanotubes (CNTs) such as the long-term toxicity and poor biodegradability [22]. Therefore, for the first time, we study a novel artificial electroconductive PLA filament for the preparation of a porous scaffold using the FDM technique. The biological and mechanical properties have been investigated to compare with the micromechanical modeling results.

## MATERIALS AND METHODS

### Material preparation

An industrial electroconductive PLA-based filament was purchased. The filament was inserted into an FDM printing machine with relatively low melting temperature, low warp properties,

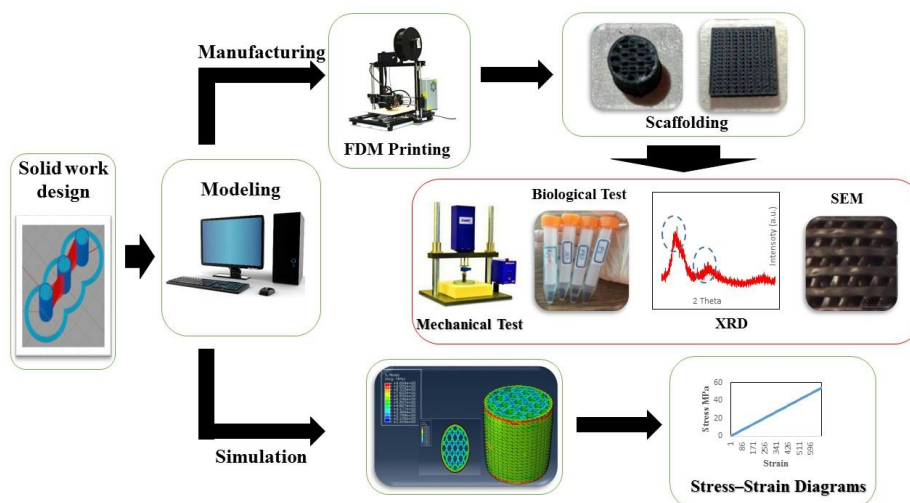


Fig 1. Schematic view of scaffold fabrication processing and investigating analysis

and biodegradable with 1.75 mm thicknesses used for scaffold preparation. The mechanical and physical properties of electroconductive-PLA (EC-PLA) filament shown in Table 1. At the glass transition temperature, the polymer changes technically from a solid to a rubber. As a result, the strength of PLA parts reduced when used above this temperature. At the melting temperature (melting range), the viscosity drops dramatically, and the polymer can be pushed through a nozzle. Therefore, it is better to use EC-PLA at a certain melting point.

#### Design of scaffold architecture

To design the scaffolds with different shapes of porous (Hexagonal, cylindrical, and cubic shape) with a density of 60%, the solid work tools were used. The hexagonal shape selected for further study due to the angles involved and the study on stress concentration is of great importance in scaffold preparation to avoid crack propagation. Honeycomb shape also involves compacted six-fold in the planer view and avoids the unwanted irregular porosity. Fig 1 shows the schematic of the design and fabrication of a porous scaffold using solid work software and an FDM printer. Honeycomb model with (D×H) equal to (5×7) mm<sup>2</sup>, cylindrical shape with (L×W×H) equal to (15×15×1) mm<sup>3</sup>, and cubic shape particularly were modeled and fabricated using solid work and FDM tools in which the D is diameter of cylinder, and L stands for the length, W is the width and H is the height of scaffolds. Fig 2 shows the cylindrical and

cubic shape of the 3D designed structures with honeycomb porosity. Both designed shapes were fabricated and designed with 65-70% porosity with nozzle temperatures ranging from 190°C-220°C.

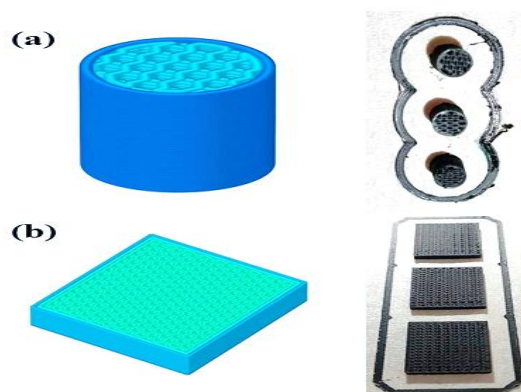


Fig 2. Porous scaffolds (a) cylindrical shape configuration with dimensions of (5 × 5 × 5) mm, (b) cubes shape with a diameter of (15×15×1) mm

#### Scaffold fabrication using fused deposition modeling (FDM)

The FDM machine was used (PARMAN Shop-Iran) with EC-PLA filament for this study. The FDM has low cost, high speed, and simplicity, which makes the process of design and fabrication of complex shapes easier. In this process, a continuous electroconductive filament (ECF) fed into the nozzle by a pinch roller mechanism, then heated under computer control up to 215°C to reach semi-liquid and then extruded on the hot

platform. The nozzles sequentially pressed to the printing platform. A computer-aided-design (CAD) approach to build 3D microstructures and then melted layer by layer to complete the model construction. Nozzle diameter, deposition rate, path spacing of the same layer, and layer thickness was 0.4 (mm), 200 (mm/min), 0.36 (mm) and 100 ( $\mu\text{m}$ ), respectively.

### **Scaffold characterization**

#### **Phase analysis**

The XRD analysis was used with Philips, Model PW-3040 with  $\text{CuK}\alpha$  radiation at 40 kV, 30mA, step size of  $0.05^\circ(2\theta^\circ)$ , and time per step 1 sec. The XRD pattern was tested before and after the fabrication of EC-PLA filament to compare the heating rate during the fabrication process.

#### **Morphology analysis**

To evaluate the morphology and geometry of the porous size, the scanning electron microscope (SEM) tools were used. Specimens were stoking to carbon binder and placed on space holder. Then coated with 5 (nm) gold by chemical vapor deposition (CVD) technique and imaged under scanning electron microscopy (Advanced Materials Research Centre, Islamic Azad University of Najafabad, Philips XI30, Netherland). The SEM images allowed us to observe differences of pores designed scaffolds and those after the fabrication process with grain size changes. Besides, after that, the samples soaking in different solutions to evaluate the degradations and apatite formation to monitor the apatite particle formation on scaffold surfaces.

#### **Mechanical testing**

The compressive test of the cylindrical scaffold was tested using a universal testing machine (Hounsfield, H50KS. UK at Isfahan University of Technology, materials engineering department) under a compression rate of 0.5 (mm/min) in terms of compressive modulus and stress-strain evaluation. Three cylindrical samples used to evaluate average along with their standard deviation ( $SD \pm 3$ ). Then, the ABAQUS simulation was applied to model and compare experimental and analytical results.

#### **Biological testing**

To investigate the apatite mineralization ability of EC-PLA scaffolds in the biological

environment as *in vitro*, samples were soaked into Simulated Body Fluid (SBF) according to Bohner and Lemaître [23], Phosphate Buffer Saline (PBS) and Ringer solutions under incubator at  $37^\circ\text{C}$  at constant pH 7.0-7 for 14 days. The SEM tools observed the apatite formation on the surfaces of scaffolds using ImageJ for the determination of porosity percentage. The pH values of the solution measured by using an electrolyte type pH meter without refreshment of the immersion. After this soaking time, the scaffolds dried at room temperature for one day, and the final weight of each sample accurately measured to an evaluated weight loss of scaffolds. The samples were prepared for cell culture evaluation in which they were washed three times in PBS for sterilization and dried in a flow chamber before cell culture. The osteoblasts cells (HuGu cells) were isolated from human dental gums. The culture medium was set using Dulbecco's Modified Eagle's Medium (DMEM) with fetal bovine serum (FBS) content in a polystyrene 2-well container. The cells in which were removed after 4 hours with washing 2 times with PBS and replacing the culture medium. The cytotoxicity is recognized for biocompatibility analysis of bone scaffold. Therefore, the positive response to cytotoxicity shows a lack of biodegradability whereas a negative response represent no toxicity behaviour.

#### **Porosity evaluation**

The porous scaffolds porosity was assessed based on void volumes determined by apparent densities [19]. Void fraction Eq. (1) is a measure of space in a material, and is a fraction of the volume of voids over a specified total volume (Eq. 1-2).

$$\text{Void Fraction} = 1 - (\rho_a - \rho_p) \quad \text{Eq. (1)}$$

$\rho_a$  and  $\rho_p$  are apparent and particle densities, respectively.

The density of PLA filament from the manufacturer company was obtained were  $1.25 \text{ gr/cm}^3$ . Apparent density ( $\rho_a$ ) for each specimen calculated by:

$$\rho_a = m_s / V_s \quad \text{Eq. (2)}$$

$m_s$  is the weight of the scaffold, and  $V_s$  is the total volume of a porous scaffold.

### **RESULT AND DISCUSSION**

The results of the X-ray diffraction test (XRD) for EC-PLA filament are plotted in Fig 3. This Fige shows there is no crystallinity phase before fabrication, which shows a higher rate

of degradation in comparison with the other crystallite materials.

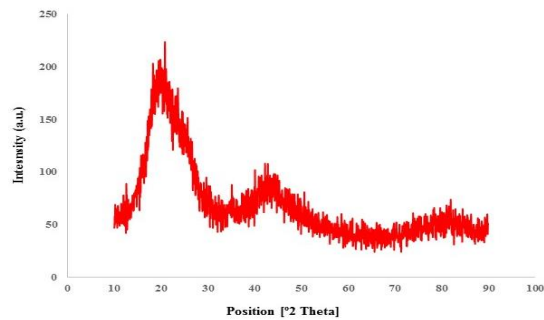


Fig 3. XRD patterns of electroconductive PLA filament used in the current study

There is a diffraction peak in a range for  $2\theta$  between  $15^\circ$  to  $30^\circ$  and  $40^\circ$  to  $50^\circ$ , which indicates a lower distance between layers and is to the reflection of atoms and a sign of amorphous material. Comparing these results with the results of the XRD pattern has shown in Fig 4, it can be concluded that there are no significant changes in the XRD pattern after the deposition of EC-PLA with several shapes.

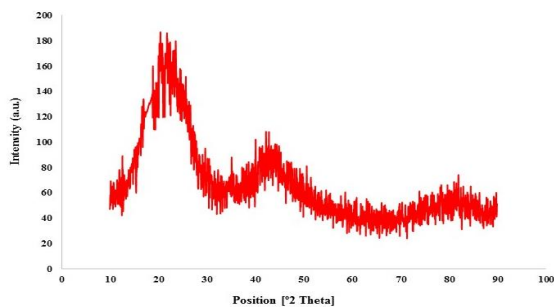


Fig 4. XRD patterns of EC-PLA filament after fusion in the 3D printing machine

The XRD pattern shows that the HA particles are in the nanosize dimension and have nanocrystalline shape below 100 nm. In addition, the apatite layer deposited on the scaffold surface with cauliflower nanostructure less than 150 nm (as shown in Fig 3 and Fig 6). Therefore, it shows that the following temperature does not change the phase of the EC-PLA before and after printing. Fig 5(a-d) shows fabricated scaffolds using an FDM printer with different shapes and porosity values. Each of these four types of pores has its own advantages and disadvantages, which shall be investigated in comparison with the others. For example, in sample (a) with a hexagonal shape, we obtain more porosity, which we demand to enable

the stem cells to grow easier and faster.

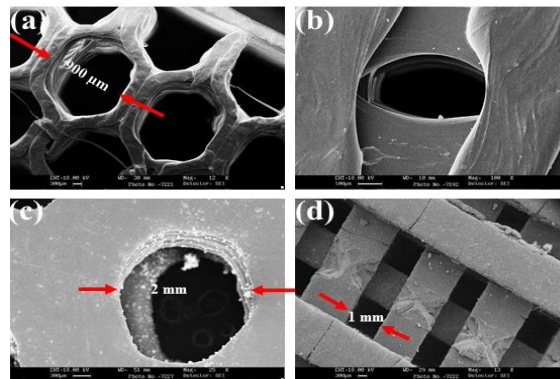


Fig 5. SEM images of 3D scaffolds using FDM printer with (a) hexagonal (b) compacted cylindrical hexagonal, (c) spherical and (d) cubic shape of pores microstructure

In sample (b), despite the less porosity, we estimate having excellent mechanical properties due to the multi-layer structure of the scaffold, which can show more mechanical strength in all directions plus good bonding with cells at the sharp edges of the layers. But the tight pores elevates the risk of failure in the weak bone tissues right at both sides of each pore.

In sample (c) with the largest pore sizes with cylindrical-shaped holes, we estimate to have the weakest bindings between the tissue and the scaffold due to the lack of sharp-edged, but the uniform, homogenous and axisymmetric structure of the scaffold, we may face an acceptable mechanical strength of the scaffold in all directions with strong tissue growth inside the pores.

The sample (d) with the cubic and multi-layered pore structure will intend to a perfect and strong binding with the growing tissue, due the sharp edges in different directions in each layer but we may face a severe weakness in the scaffold resistance against shear stresses according to the cross layers of scaffold strip elements hardly to believe in acting as a moment frame structure in shear loadings. Different magnification images were obtained to investigate the morphology of porous architecture with a cylindrical and hexagonal shape.

Fig 5(c) shows the 2 mm diameter of the cylindrical porous shape in which several layers were stood together to create this pore. All the pores were connected and the throats of EC-PLA measured using ImageJ.

The porosity value, size, geometry, orientation, and open porosity in nutrients transportation for

Table 1. Mechanical and physical properties of EC-PLA used in this study

Quantity	Glass transition temperature	Melting temperature	Elastic modulus (MPa)	Tensile strength (MPa)	Elongation (%)	Bending strength (MPa)	Impact strength (J/cm)	Density (Kg/m <sup>3</sup> )
EC-PLA	± 55°C	175°C	350 - 280	10 - 60	1.5 - 380	0.89 - 1.03	0.16 - 1.35	1210 - 1430

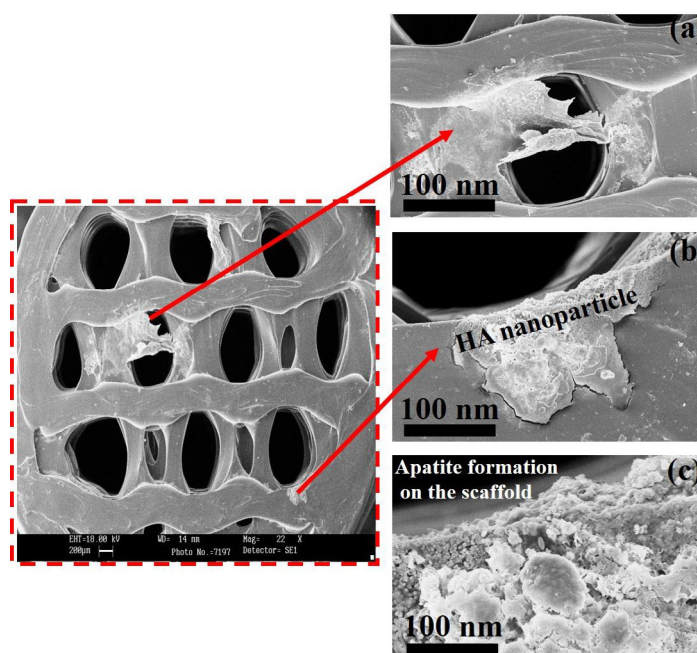


Fig 6. SEM images of scaffolds fabricated using FDM technique coated with HA nanoparticle soaked in the biological (a) the cylindrical shape, (b) the apatite formation on the scaffold, and (c) the precipitation of apatite on the HA coats

the growth of cells and new tissue is essential and vital [24, 25]. An ideal scaffold must have open and free porosity with an interconnected architecture. Electroconductive scaffolds were coated with HA bioceramic nanoparticles to enabled the ability to grow new bone tissue upon implantation and establish a strong bond between the implant and the bone. In this study, the hydroxyapatite was used to enhance the chemical composition and structure of the scaffold surface to increase the similarity of the inorganic part of the bone with organic components. In other words, the HA nanoparticle shows non-toxic with stimulates osteogenesis response and causes the bone to grow into pores cite. As a result, due to the biocompatibility properties of HA, with bone, it is the best substitute for hard body tissues as bone substitute or coating on a scaffold. A comparison of Fig 5(a) and 5(b) shows that best and strength architecture belongs to hexagonal shape. However, the size of the hole may effect

on compression strength of the component. A high percentage of large porosity results in a reduction in the mechanical strength of the scaffold. Therefore, creating a balance between the properties mentioned can lead to the creation of a suitable scaffold for use in tissue engineering [26, 27]. Fig 6(a-c) shows a single porous type of compacted cylindrical hexagonal architecture with a different micrometer (Hexagonal porous shape) and millimeter (spherical and cubic porous shape) that let nutrients and proteins pass through the tissue. The hexagonal porous shape involved low-stress concentration on its sides, which prevents crack propagation. The apatite formation process of the coated sample with HA on the scaffold not only depends on the chemical properties of the surface but also depends on the adhesion between the scaffold and coat as shown in Fig 6(a-c). The prepared scaffolds should not cause an inflammatory reaction, any immunogenicity, cytotoxicity, and degradation rate related to

tissue growth. Thus, the simulated body fluid and ringer solution with standard mixture selected to evaluate the degradation rate and apatite formation of EC-PLA scaffolds. The pH value increased with the soaking time to 8, in which the calcium present in HA shows alkalinity reaction in SBF and ringer solution.

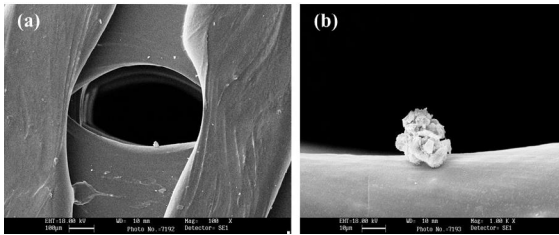


Fig 7. SEM images of biological response and apatite formation of cylindrical scaffold after soaking in PBS solution, a) Cavity creature of honeycomb shape porosity, and b) magnifies of cauliflower apatite particle

Fig 7(a-b) illustrates SEM images of the biological response of EC-PLA scaffolds after soaking in SBF, PBS, and Ringer, respectively. Apatite particles observed around and inside of scaffold cavities with cauliflower morphology. Some white points are seen in images that are likely to contaminate the surface of the sample. Fig 8 (a-b) shows cell growth and the reaction of cells on the surface of the scaffolds after 24 h in the culture medium.

The adhesion between the cell and the scaffold surface, which contains the bioactive coating affixed to the electroconductive scaffold represented in Fig 8b.

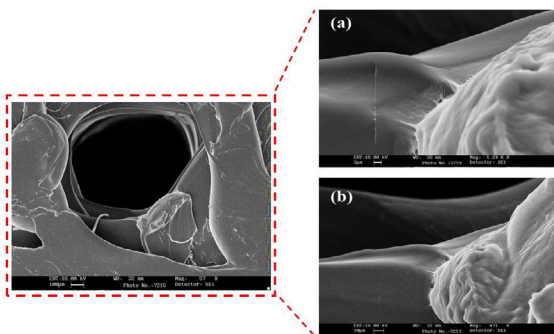


Fig 8. SEM images of biological response and apatite formation of cylindrical scaffold after soaking in Ringer solution with different magnification (a & b)

Figure 9 shows the comparison of compressive strength and fracture toughness before and after soaking in biological solutions (PBS and SBF) indicated that fluctuation is between 30 to 40 MPa.

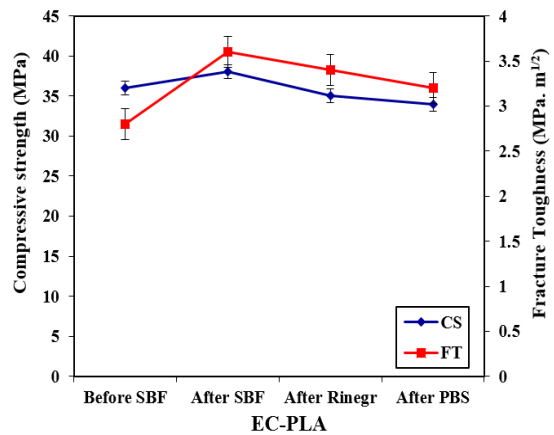


Fig 9. Compressive strength changes of electroconductive PLA before and after soaking in SBF, Ringer and PBS solution

Figure 9 shows that the compressive strength of the scaffold has an increasing trend in the SBF solution; however, it has a decreasing trend after soaking in ringer saline. Also, similar behavior occurred for the fracture toughness value as it is shown in Figure 9; the fracture toughness of the scaffold measured in the stress-strain evaluation, which is the area under the stress-strain diagram before and after soaking in the biological saline.

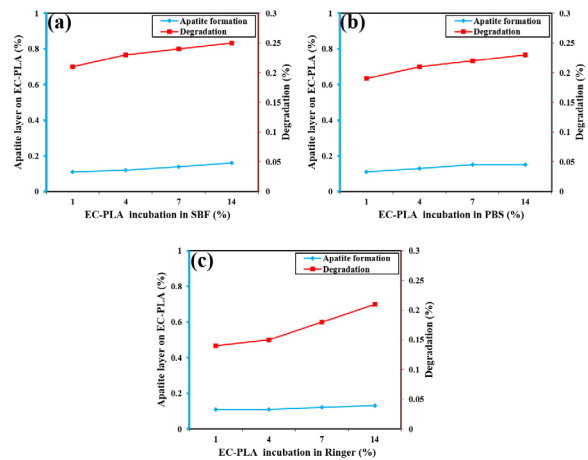


Fig 10. EC-PLA degradation due to appetite formation in biological solution such as (a) SBF, (b) PBS and (c) ringer solution

Figure 10 (a-c) shows the apatite formation and degradation rate of the coated sample with HA nanoparticle after soaking in three various medium for 14 days.

The obtained results show that the samples with different architecture have an increasing apatite formation rate constantly. However, the degradation rate dramatically increases after the first week which depends on the high degradation

rate of HA in the SBF saline.

Fig 11 also presents the porosity value of electroconductive PLA before and after incubation. In all three solutions, the porosity remains high, in the range of 60-70%, which is a high amount in preparation of scaffold for bone substitute purposes. Also, Fig 11 shows that the pore size of the coated sample decreased with soaking in the SBF for the cubic sample.

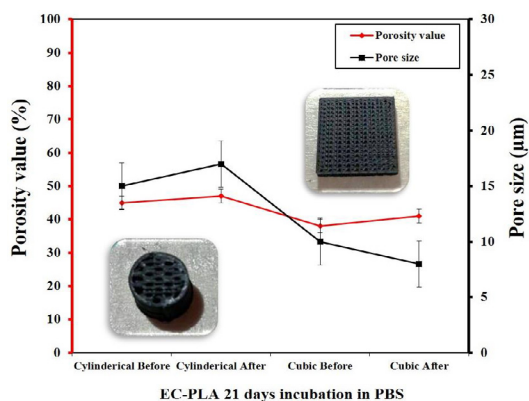


Fig 11. Porosity value alteration of electroconductive PLA before and after soaking in the SBF and PBS solution

However, the sample with cylindrical shape obtains higher pore size in their architecture after submerged in the SBF solution. The stress-strain curve of cylindrical scaffold after compression test analysis shown in Fig 12.

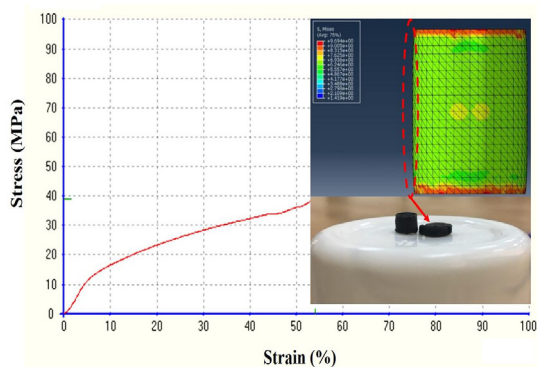


Fig 12. Diagram of stress-strain of cylindrical scaffold after compressive test analysis

Maximum strength at 50 percent of strain was 39.14 MPa before soaking in solution for 14 days in samples with porous honeycomb shape. It can be concluded that the compressive strength of EC-PLA increased besides to forces and remain constant with changing its architecture. In this study, the index of strength multiplied to total

porosity (39.14×70%), introduced as a valuable index. As strength and porosity are two favorable and essential characteristics for scaffolds in tissue engineering applications, so the design of the scaffold in the SolidWorks software carried out with a porosity of 70%, and then the model transferred to Abaqus software. In this work, general static loading was determined in the Abaqus software. According to the information obtained from compressive strength evaluation, the Poisson ratio set as 0.33 and the elastics modulus was near 2.17 GPa and the filament density set up on 1.25±0.25 (g/cm<sup>3</sup>). After applying the mechanical properties of the material to the bone scaffold, all the boundaries of the surface tied to the scaffold. To verify the final compressive resistance of the scaffold, the vertical force of 100-150 KN applied to the top of the scaffold region. The Tet mode was set for the scaffold as meshing and then the analysis process performed. The analytical results of the scaffold showed that by applying force to the scaffold at its most sensitive point, the 9.7± 2 MPa Von Mises stress (VMS) could withstand the scaffold mentioned above. The barrels' shape in the scaffold was predictable due to its cylindrical way which can support the obtained results. Fig 13 shows the explanation of the tension and compression of cylindrical shape with honeycomb inside structure loaded with 100-150 KN. The obtained results from the experimental outcome derived into Abaqus simulation, which indicated the advantages of cylindrical forms compared to other models. Investigation of cross-section and internal parts of the scaffolds described the ultimate tensile strength that occurred on the edge of the porous cylinder. Besides, one can say the most tensions were also on the outer edges of the scaffold. This simulation analysis confirms that the EC-PLA scaffold with HA coating can be mechanically acceptable. In this work, the limitation was the creation of collagen in which the biggest problem is its high cost and low production centers. Therefore, one can introduce a gelatin biopolymer as a perfect alternative to collagen. Gelatin has good biocompatibility and good bone mineralization feature. The distribution of the HA nanoparticles deposited on a porous 3D printed scaffold was suitable with the low rate of agglomeration of the HA. The elastic modulus of the ideal scaffolds was measured, ranging from 30-40 MPa for the experimental sample; however, the Abaqus software represents 50-60 MPa for a

similar sample, as shown in Fig 13. As it is shown in Fig 13, the sample with hexagonal shape coated with HA nanoparticle is almost completely disintegrated, while other structure remains completely intact. Normally, cortical bones have a compressive strength of 110 to 150 MPa and an elastic modulus of 18 to 22 GPa, whereas the spongy bones have a compressive strength of 2 to 6 MPa and an elastic modulus of 0.1 to 0.3 GPa [28-32].

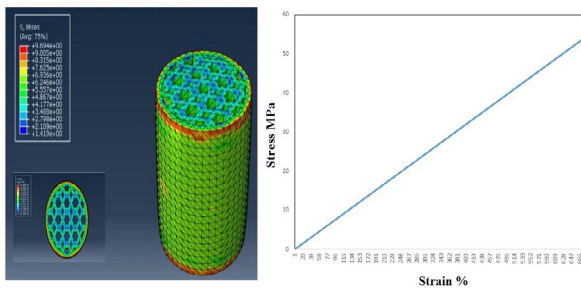


Fig 13. Simulation of cylindrical architecture with hexagonal structure with ABAQUS software for scaffold prepared by FDM technology using for bone substitute

The mechanical strength of magnetic composite scaffolds is one of the most important characteristics of the performance and quality of this bone substitute using for photothermal therapy approaches as a novel magnetic bifunctional nanocomposite [33-39]. After insertion of scaffolds into the *in vitro* medium, as soon as the bone is implanted, this new tissue is affected by different loads from different directions. As the mechanical loads are not tolerated in the scaffold structure, the bony scaffold may shortly crack and subsequently fail [40-43]. This strength is related to several factors such as the material properties, their strength, the type of reinforcement, mineral particles and their geometry [44-48]. The results of the MTT assay show the effect of EC-PLA composite bone growth on the growth and proliferation of osteoblasts cells. None of the doses used in this study caused cytotoxicity for all cell lines. The results show that the EC-PLA scaffold coated with HA nanoparticles represents biocompatible behavior in the HuGu cell types. Regarding the shape, it can be said that the growth and proliferation of cell proliferation have been associated with time, which is observed in all four bio-nano composite samples. On the first day of culture, there was a significant difference between the number of cells in different samples. Providing a suitable substrate for cell growth is the

most important and effective reason for increasing cell growth in the presence of scaffolds. It can be said that by increasing the HA nanoparticles coated on the EC-PLA, the cell viability increased.

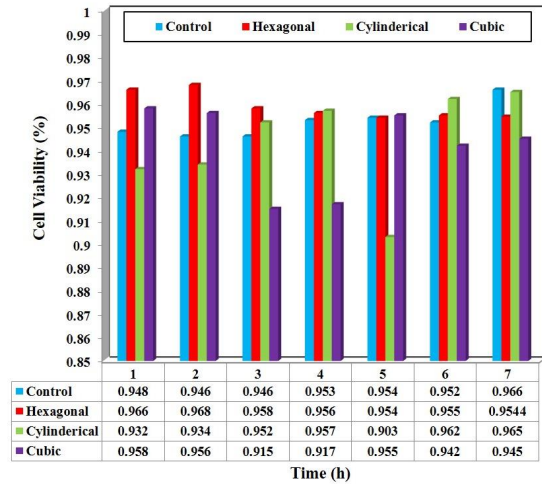


Fig 14. Percentage of cell viability and proliferation on the bone scaffold after 7 hours incubation of hexagonal, cylindrical and cubic structure

Fig 14 was performed on four samples with different 3D printing microstructure coated with HA nanoparticle in which each sample was exposed to HuGu osteoblasts cells with 0.03 mg/ml. The observation shows that any doses used in this study had a cytotoxic response for the HuGu cell line. It can be concluded that the scaffolds fabricated using FDM technology were compatible with HuGu osteoblasts cells. Also, Fig 14 shows the results of the MTT assay and the rate of proliferation and growth of stem cells in contact with electroconductive scaffolds coated with hydroxyapatite ceramic. The conclusion that can be drawn at first glance is the growth and proliferation of cells overtime for 7 and 14 hours, which is observed in the control sample and all four bio-coated samples. In the first, second and third days of cell culture, there was a significant difference between the number of cells in different samples. However, due to the high porosity value of about 75%, the cells were sometimes larger than the control sample. Fabrication of a scaffold with a conductive substrate can cause cells to grow better in a cell line with a porosity of more than 1 micron. An interesting result of this study is the enhancement of the growth and viability of stem cells on scaffolds with hexagonal structure coated with hydroxyapatite nanoparticles in the SBF saline.

## CONCLUSION

Additive manufacturing can produce porous scaffolds with different shapes and various microstructure. In the present study, the EC-PLA filament was used by the FDM 3D printer machine. Cubic and cylindrical structural shapes with honeycomb internal layering designs were chosen to fabricate artificial scaffolds. The amount of total porosity was 70-75%, as designed and remained high between (60-70%) after soaking the samples in the solutions, which was a high amount for a porous scaffold in tissue engineering. The SEM images indicated the formation of apatite on the surface of porous scaffolds after 14 days soaking could provide suitable bioactivity. The compressive strength of the hexagonal structure measured 39.14 MPa. The index of strength multiplied by total porosity was equal to 2740, which is very high compared to other materials like ceramics. Rate of degradation due to apatite formation increased during soaking in SBF, PBS, and ringer solutions which shows an increase in biocompatible value. Also, the ABAQUS simulation applied to the designed scaffold. The obtained results indicated the suitability of the toughness of EC-PLA scaffolds and confirmed that the EC-PLA scaffold is mechanically acceptable.

## REFERENCES

1. Saber-Samandari S, & Gross K A. Micromechanical properties of single crystal hydroxyapatite by nanoindentation. *Acta Biomater.* 2009; 5(6), 2206-2212.
2. Heydari H A, Karamian E, Poorazizi E, Heydaripour J, Khandan A. Electrospun of polymer/bioceramic nanocomposite as a new soft tissue for biomedical applications. *Asian Ceram. Soc.* 2015; 3(4), 417-425.
3. Moghadas B K, Akbarzadeh A, Azadi M, Aghili A, Rad A S, Hallajian S. The morphological properties and biocompatibility studies of synthesized nanocomposite foam from modified polyethersulfone/graphene oxide using supercritical CO<sub>2</sub>. *J Macromol Sci A.* 2020; 1-10.
4. Kamyab Moghadas B, Azadi M. Fabrication of Nanocomposite Foam by Supercritical CO<sub>2</sub> Technique for Application in Tissue Engineering. *J Tiss Mater.* 2019; 2(1), 23-32.
5. Aghdam H A, Sanatizadeh E, Motiffard M, Aghadavoudi F, Saber-Samandari S, Esmaili S, Khandan A. Effect of calcium silicate nanoparticle on the surface feature of calcium phosphates hybrid bio-nanocomposite using for bone substitute application. *Powder Technol.* 2020; 361, 917-929.
6. Costantini M, Colosi C, Mozetic P, Jaroszewicz J, Tosato A, Rainer A, Barbeta A. Correlation between porous texture and cell seeding efficiency of gas foaming and microfluidic foaming scaffolds. *Mat Sci Eng C-Mater.* 2016; 62, 668-677.
7. Farazin A, Aghdam H A, Motiffard M, Aghadavoudi F, Kordjamshidi A, Saber-Samandari S, Khandan A. A polycaprolactone bio-nanocomposite bone substitute fabricated for femoral fracture approaches: Molecular dynamic and micro-mechanical Investigation. *J Nanoanaly.* 2019.
8. Tahririan M A, Motiffard M, Omidian A, Aghdam H A, Esmaeali A. Relationship between bone mineral density and serum vitamin D with low energy hip and distal radius fractures: A case-control study. *Arch Bone Joint Surg.* 2017; 5(1), 22.
9. Kordjamshidi A, Saber-Samandari S, Nejad M G, Khandan A. Preparation of novel porous calcium silicate scaffold loaded by celecoxib drug-using freeze-drying technique: Fabrication, characterization and simulation. *Ceram Int.* 2019; 45(11), 14126-14135.
10. Datta S, Das A, Sasmal P, Bhutoria S, Roy Chowdhury A, Datta P. Alginate-poly (amino acid) extrusion printed scaffolds for tissue engineering applications. *Int J Polym Mater Po.* 2020; 69(2), 65-72.
11. Esmaili S, Shahali M, Kordjamshidi A, Torkpoor Z, Namdari F, Samandari S S, Khandan A. An artificial blood vessel fabricated by 3D printing for pharmaceutical applications. *Nanomed J.* 2019; 6(3), 183-194.
12. Esmaili S, Aghdam H A, Motiffard M, Saber-Samandari S, Montazeran A H, Bigonah M, Khandan A. A porous polymeric-hydroxyapatite scaffold used for femur fractures treatment: fabrication, analysis, and simulation. *Eur J Orthop Surg Traumatol.* 2020; 30(1), 123-131.
13. Esmaili S, Khandan A, Saber-Samandari S. Mechanical performance of three-dimensional bio-nano composite scaffolds designed with digital light processing for biomedical applications. *Iran J Med Phys.* 2018; 15, 328-328.
14. Khandan, A., & Ozada, N. Bredigite-Magnetite (Ca<sub>7</sub>MgSi<sub>4</sub>O<sub>16</sub>-Fe<sub>3</sub>O<sub>4</sub>) nanoparticles: A study on their magnetic properties. *J Alloy Compd.* 2017; 726, 729-736.
15. Khandan A, Ozada N, Saber-Samandari S, Nejad M G. On the mechanical and biological properties of bredigite-magnetite (Ca<sub>7</sub>MgSi<sub>4</sub>O<sub>16</sub>-Fe<sub>3</sub>O<sub>4</sub>) nanocomposite scaffolds. *Ceram Int.* 2018; 44(3), 3141-3148.
16. Serra T, Planell J A, Navarro M. High-resolution PLA-based composite scaffolds via 3-D printing technology. *Acta biomater.* 2013; 9(3), 5521-5530.
17. Stoppato M, Carletti E, Sidarovich V, Quattrone A, Unger R E, Kirkpatrick C J, Motta A. Influence of scaffold pore size on collagen I development: a new in vitro evaluation perspective. *J Bioact Compat Pol.* 2013; 28(1), 16-32.
18. Giordano R A, Wu B M, Borland S W, Cima L G, Sachs E M, Cima M J. Mechanical properties of dense polylactic acid structures fabricated by three-dimensional printing. *J Biomat Sci, Polymer Edition.* 1997; 8(1), 63-75.
19. Velioglu Z B, Pulat D, Demirbakan B, Ozcan B, Bayrak E, Eriskan C. 3D-printed poly (lactic acid) scaffolds for trabecular bone repair and regeneration: scaffold and native bone characterization. *Connect Tissue Res.* 2019; 60(3), 274-282.
20. Fafenrot S, Grimmelsmann N, Wortmann M, Ehrmann A. Three-dimensional (3D) printing of polymer-metal hybrid materials by fused deposition modeling. *Mater.* 2017; 10(10), 1199.
21. Sahmani S, Saber-Samandari S, Shahali M, Yekta H J, Aghadavoudi F, Montazeran A H, Khandan A. Mechanical and biological performance of axially loaded novel bio-nano composite sandwich plate-type implant coated by biological polymer thin film. *J Mech Behav Biomed.* 2018;

- 88, 238-250.
22. Kenry L W, Loh K P, Lim C T. When stem cells meet graphene: opportunities and challenges in regenerative medicine. *Biomaterials*. 2018; 155, 236-250.
  23. Bohner M, Lemaire J. Can bioactivity be tested in vitro with the SBF solution?. *Biomaterials*, 2009; 30(12), 2175-2179.
  24. Monfared R M, Ayatollahi M R, Isfahani R B. Synergistic effects of hybrid MWCNT/nano-silica on the tensile and tribological properties of woven carbon fabric epoxy composites. *Theor Appl Fract Mec*. 2018; 96, 272-284.
  25. Moradi-Dastjerdi R, Behdinin K. Stability analysis of multifunctional smart sandwich plates with graphene nanocomposite and porous layers. *Int J Mech Sci*. 2020; 167, 105283.
  26. Khandan A, Jazayeri H, Fahmy M D, Razavi M. Hydrogels: Types, structure, properties, and applications. *Biomater Tissue Eng*. 2017; 4(27), 143-69.
  27. Ayatollahi M R, Moghimi Monfared R, Barbaz Isfahani R. Experimental investigation on tribological properties of carbon fabric composites: effects of carbon nanotubes and nano-silica. *P I Mech Eng L-J Mat*. 2019; 233(5), 874-884.
  28. Montazeran A H, Saber Samandari S, Khandan A. Artificial intelligence investigation of three silicates bioceramics-magnetite bio-nano composite: Hyperthermia and biomedical applications. *Nanomed J*. 2018; 5(3), 163-171.
  29. Joneidi Yekta H, Shahali M, Khorshidi S, Rezaei S, Montazeran A H, Samandari S, Khandan A. Mathematically and experimentally defined porous bone scaffold produced for bone substitute application. *Nanomed J*. 2018; 5(4), 227-234.
  30. Barbaz-I R. Experimental determining of the elastic modulus and strength of composites reinforced with two nanoparticles (Doctoral dissertation, MSc Thesis, School of Mechanical Engineering Iran University of Science and Technology, Tehran, Iran); 2014.
  31. Karamian E, Nasehi A, Saber-Samandari S, Khandan A. Fabrication of hydroxyapatite-baghdadite nanocomposite scaffolds coated by PCL/Bioglass with polyurethane polymeric sponge technique. *Nanomed J*. 2017; 4(3), 177-183.
  32. Khandan A, Karamian E, Bonakdarchian M. Mechanochemical synthesis evaluation of nanocrystalline bone-derived bioceramic powder using for bone tissue engineering. *Dent Hypoth*. 2014; 5(4), 155.
  33. Salami MA, Kaveian F, Rafienia M, Saber-Samandari S, Khandan A, Naeimi M. Electrospun polycaprolactone/lignin-based nanocomposite as a novel tissue scaffold for biomedical applications. *J. Medical Signals Sens*. 2017; 7(4), 228.
  34. Khandan A, Karamian E, Mehdikhani-Nahrkhalaji M, Mirmohammadi H, Farzadi A, Ozada N, Zamani K. Influence of spark plasma sintering and baghdadite powder on mechanical properties of hydroxyapatite. *Proce Mat Sci*. 2015; 11, 183-189.
  35. Ghayour H, Abdellahi M, Nejad M G, Khandan A, Saber-Samandari S. Study of the effect of the Zn<sup>2+</sup> content on the anisotropy and specific absorption rate of the cobalt ferrite: the application of Co<sub>1-x</sub>Zn<sub>x</sub>Fe<sub>2</sub>O<sub>4</sub> ferrite for magnetic hyperthermia. *J Aust Ceram Soc*. 2018; 54(2), 223-230.
  36. Sahmani S, Shahali M, Nejad M G, Khandan A, Aghdam MM, Saber-Samandari S. Effect of copper oxide nanoparticles on electrical conductivity and cell viability of calcium phosphate scaffolds with improved mechanical strength for bone tissue engineering. *Eur Phys J Plus*. 2019; 134(1), 7.
  37. Sahmani S, Khandan A, Esmaeili S, Saber-Samandari S, Nejad M G, Aghdam MM. Calcium phosphate-PLA scaffolds fabricated by fused deposition modeling technique for bone tissue applications: Fabrication, characterization, and simulation. *Ceram Int*. 2020; 46(2), 2447-2456.
  38. Wibowo A, Vyas C, Cooper G, Qulub F, Suratman R, Mahyuddin A I, Bartolo P. 3D Printing of Polycaprolactone-Polyaniline Electroactive Scaffolds for Bone Tissue Engineering. *Materials*, 2020; 13(3), 512.
  39. Potnuru A, Tadesse Y. Investigation of polylactide and carbon nanocomposite filament for 3D printing. *Prog Add Manu*. 2019; 4(1), 23-41.
  40. Amanjani A R, Zandi R, Samandari S S. Determination of anterior femoral bowing to length ratio in Iranian population. *Pajoohandeh J*. 2020; 24(1), 0-0.
  41. Saber-Samandari S, Mohammadi-Aghdam M, Saber-Samandari S. A novel magnetic bifunctional nanocomposite scaffold for photothermal therapy and tissue engineering. *Int J Biol Macromol*. 2019; 138, 810-818.
  42. Bidgoli M R, Alemzadeh I, Tamjid E, Khafaji M, Vossoughi M. Fabrication of hierarchically porous silk fibroin-bioactive glass composite scaffold via indirect 3D printing: Effect of particle size on physico-mechanical properties and in vitro cellular behavior. *Mat Sci Eng C-Mater*. 2019; 103, 109688.
  43. Maghsoudlou M A, Nassireslami E, Saber-Samandar S, Khandan A. Bone regeneration using bio-nanocomposite tissue reinforced with bioactive nanoparticles for femoral defect applications in medicine. *Avicenna J. Med. Biotechno*. 2020; (2).
  44. Maghsoudlou M A, Isfahani R B, Saber-Samandari S, Sadighi M. Effect of interphase, curvature, and agglomeration of SWCNTs on mechanical properties of polymer-based nanocomposites: Experimental and numerical investigations. *Compos Part B-Eng*. 2019; 175, 107119.
  45. Tamjidi S, Esmaeili H, Moghadas B K. Application of magnetic adsorbents for the removal of heavy metals from wastewater: a review study. *Materials Research Express*. 2019; 6(10), 102004.
  46. Rad A S, Samipour V, Movaghgharnezhad S, Mirabi A, Shahavi M H, Moghadas B K. X12N12 (X= Al, B) clusters for protection of vitamin C; molecular modeling investigation. *Surf Interf*, 2019; 15, 30-37.
  47. Shokri-Oojghaz R, Moradi-Dastjerdi R, Mohammadi H, Behdinin K. Stress distributions in nanocomposite sandwich cylinders reinforced by aggregated carbon nanotube. *Polym Composite*. 2019; 40(S2), E1918-E1927.
  48. Pourasghar A, Moradi-Dastjerdi R, Yas M H, Ghorbanpour Arani A, Kamarian S. Three-dimensional analysis of carbon nanotube-reinforced cylindrical shells with temperature-dependent properties under thermal environment. *Polym Composite*. 2018; 39(4), 1161-1171.